

Motion estimation of a rigid body with an EKF using magneto-inertial measurements

Charles-Ivan Chesneau, Mathieu Hillion, Christophe Prieur

▶ **To cite this version:**

Charles-Ivan Chesneau, Mathieu Hillion, Christophe Prieur. Motion estimation of a rigid body with an EKF using magneto-inertial measurements. IPIN 2016 - 7th Conference on Indoor Positioning and Indoor Navigation, Oct 2016, Madrid, Spain. pp.1 - 6, 10.1109/IPIN.2016.7743702 . hal-01448486

HAL Id: hal-01448486
https://hal.science/hal-01448486

Submitted on 28 Jan 2017

HAL is a multi-disciplinary open access archive for the deposit and dissemination of scientific research documents, whether they are published or not. The documents may come from teaching and research institutions in France or abroad, or from public or private research centers.

L'archive ouverte pluridisciplinaire **HAL**, est destinée au dépôt et à la diffusion de documents scientifiques de niveau recherche, publiés ou non, émanant des établissements d'enseignement et de recherche français ou étrangers, des laboratoires publics ou privés.

Motion estimation of a Rigid Body with an EKF using Magneto-Inertial Measurements

Charles-Ivan Chesneau*, Mathieu Hillion* and Christophe Prieur†

***Abstract*— This paper studies the attitude and position estimation problem of a rigid body equipped with inertial and magnetic sensors. First a continuous-time model is provided linking the motion of the body and sensor measurements, which depend on the total magnetic field and measurement noise. The magnetic field may depend both on the space variable (since the indoor navigation is considered) and on the time variable (since power-line interference is taken into account). An Extended Kalman Filter is designed aiming at the minimization of the drifting error on the estimated position. A numerical simulation illustrates the motion estimation result. Some indoor tests are finally performed to confirm the approach and the obtained convergence on real experiments.**

I. Introduction

Outdoor motion estimation for bodies and vehicles is often based on position sensors (usually GPS) and inertial sensors. For such observation problems, there exists a large literature merging both kinds of measurements, notably by the means of the Extended Kalman Filter (EKF), as in [26], nonlinear observers (see e.g., [11], [20], [25]), and hybrid observers, as in [3], yielding attitude and position estimations. In contrast to outdoor navigation, GPS signals cannot be used for indoor navigation, requiring the use of other sensors and output signals. Therefore indoor navigation is subject to active research for observer design and various applications. The reader can refer to several surveys on techniques that have been developped, mainly relying on a dedicated or existing infrastructure to varying extent [5], [14], [15] (WLAN, UWB, RFID tags, LED,...), whereas some rely on optical or hybrid sensors [16], or consist in "pedestrian dead-reckoning" [12]. An overview of human indoor navigation techniques can be found in [9].

Among those which do not require an existing infrastructure, two techniques can be mentionned: foot-mounted dead reckoning, as implemented in [10] or [18], allows positionning in unknown environment by exploiting the nature of the movement, namely through Zero-velocity update / detection (ZUPT). It can achieve a performance level of 1% of travelled distance and below [13], [17], [23]. Magnetic fingerprinting/mapping [4], [22], [24] makes use of the geomagnetic field anomalies in order to compute a position, but requires the magnetic field to be mapped at some point.

*Charles-Ivan Chesneau and Mathieu Hillion are with Sysnav, 57 Rue de Montigny, 27200 Vernon, France charles-ivan.chesneau@sysnav.fr.

†Christophe Prieur is with Gipsa-lab, Department of Automatic Control, Grenoble Campus, 11 rue des Mathématiques, BP 46, 38402 Saint Martin d'Hères, France, christophe.prieur@gipsa-lab.fr.

Previous papers such as [27], [28] already underlined that by using MEMS[1] inertial and magnetic sensors, the magnitude and nature of magnetic disturbances found in buildings allow relatively accurate velocity estimates of a sensor board in a completely unknown environment, with no need to deploy an infrastructure, and without relying on hypothesis about the nature of the movement. This then allows trajectory reconstruction, albeit drifting. The patented technique [29] was further studied and demonstrated in [6], [7], [8] for indoor navigation. It was shown that the technique had potential applications in heavy launchers and space vehicles [19]. Finally, [2] studied observability issues that come with this technique.

In a very preliminary work [27], [28], an EKF was used to obtain experimental results, whose state was composed of 45 variables and measurement vector of more than 30 variables, combining the data of several off-the-shelf IMUs in order to compute a trajectory. The large number of parameters needed to be precisely tuned for each trajectory undermined its usability.

In [6], [7], [8], an AHRS was combined with a separate non-linear continuous-time observer to obtain a velocity estimate using only gyrometer and magnetic measurements. A theoritical proof of convergence of the latter in absence of measurement errors was provided, with a few successful experimental 3D trajectories. Accelerometer measurements were used only for attitude computation.

In this paper, a miniaturized smartphone-sized integrated sensor board is presented. A single smaller EKF observer is described with its underlying discrete-time model, and used to obtain an attitude and a velocity estimate from accelerometer, gyrometer and magnetic measurements. The observer is tuned by accounting for measured sensor uncertainties. Then, its performance is extensively evaluated as is with the same settings, both on simulated and experimental data. Experimental results show relative drift-errors under a maximum of 3.3% of travelled distance on tested closed-path trajectories, which is comparable with pedestrian dead-reckoning systems [13], [17], but achieved on completely free movements.

This paper is organized as follows. First a continuous-time model is written to describe the dynamics of the rigid body and magneto-inertial measurements. See Section II where the observation problem is also stated. Then an EKF observer is designed in Section III to tackle measurement noise and to estimate the attitude and the position. Section

[1]Microelectromechanical System

IV contains some numerical simulations, and Section V gives the results of a large series of indoor tests illustrating the observer convergence and the obtained performance in terms of estimation errors.

II. Problem statement

As in [7], let us consider the tracking of a rigid body motion, using strapdown MEMS inertial sensors and a magnetometer network.

A. Continuous-time model

Let $\mathfrak{R}$ be an inertial frame of reference. Let $\mathcal{B}_i$ be an orthonormal basis fixed with respect to $\mathfrak{R}$, and $\mathcal{B}_b$ an orthonormal basis moving with the rigid body. Let R be the rotation matrix such that its columns represent coordinates of the basis $\mathcal{B}_b$ expressed in $\mathcal{B}_i$. Coordinates of a vector are denoted using the i (resp. b) subscript if expressed in $\mathcal{B}_i$ (resp. $\mathcal{B}_b$), such that $\square_i = R\square_b$. Let q be its associated quaternion such that $q * \square * q^{-1} \equiv R\square$, with $*$ denoting the quaternion multiplication.

Rigid-body motion can be modelled by the continuous-time differential equations (1) and (2):

$$\frac{dq}{dt} = \frac{1}{2} q * \boldsymbol{\omega}_b \tag{1}$$

$$\frac{d\mathbf{v}_b}{dt} = -\boldsymbol{\omega}_b \times \mathbf{v}_b + \boldsymbol{\gamma}_b + \mathbf{g}_b \tag{2}$$

where

- q stands for the attitude quaternion,
- $\mathbf{v}$ the velocity vector in $\mathfrak{R}$ of the accelerometer point of percussion (denoted M_P) ,
- $\boldsymbol{\omega}$ the $\mathfrak{R}_b/\mathfrak{R}_i$ angular velocity vector (or its associated quaternion)
- $\boldsymbol{\gamma}$ the non-gravitational acceleration of the 3-axis accelerometer point of percussion
- $\mathbf{g}$ the gravitational acceleration vector.

Let us denote $\mathbf{x}$ the relative position of M_P from an arbitrary fixed point in $\mathfrak{R}$. Then, denoting $\frac{d\mathbf{x}}{dt}$ the time derivative of $\mathbf{x}$ in $\mathfrak{R}$:

$$\frac{d\mathbf{x}}{dt} = \mathbf{v} \tag{3}$$

Let us denote $\mathbf{B}^{(\mathrm{t})}$ the total magnetic field at a fixed point M_B of the rigid body. Assuming enough regularity of the vector field with respect to time and space, straightforward derivation yields the following equation:

$$\frac{d\mathbf{B}_b^{(\mathrm{t})}}{dt} = -\boldsymbol{\omega} \times \mathbf{B}_b^{(\mathrm{t})} + (\nabla \mathbf{B}_b^{(\mathrm{t})})(\mathbf{v}_b + \boldsymbol{\omega}_b \times \overrightarrow{M_P M_B}) + \left(\frac{\partial \mathbf{B}^{(\mathrm{t})}}{\partial t}\right)_b \tag{4}$$

where $\nabla \mathbf{B}^{(\mathrm{t})}$ is the (3x3) Jacobian of the magnetic field at M_B. If $\mathbf{B}^{(\mathrm{t})}$ is time-invariant in the inertial frame, and if $\nabla \mathbf{B}^{(\mathrm{t})}$ is available and non-singular, it can be expected that the velocity vector $\mathbf{v}$ is observable through appropriate tracking of the magnetic field and its spatial variations [6]. However in urban environment, the magnetic field is perturbed by power-line interference. Such periodic interference can be rather strong (up to $\sim$ 10mG in amplitude near a train station). This perturbation violates any working assumption that the magnetic field be time-invariant in the inertial frame.

In the following, we assume that $\mathbf{B}^{(\mathrm{t})}$ is the sum of two vector fields $\mathbf{B}^{(\mathrm{t})} = \mathbf{B} + \mathbf{B}^{(\mathrm{pl})}$ with:

- $\mathbf{B}$ the time-invariant component of the magnetic field, i.e. $\frac{\partial \mathbf{B}}{\partial t} = 0$;
- $\mathbf{B}^{(\mathrm{pl})}$ such that $\nabla \mathbf{B}^{(\mathrm{pl})} \approx 0$, modelling the periodic power line interference, implying $\nabla \mathbf{B}^{(\mathrm{t})} \approx \nabla \mathbf{B}$.

It follows

$$\frac{d\mathbf{B}_b}{dt} = -\boldsymbol{\omega}_b \times \mathbf{B}_b + (\nabla \mathbf{B}_b^{(\mathrm{t})})(\mathbf{v}_b + \boldsymbol{\omega}_b \times \overrightarrow{M_P M_B}) \tag{5}$$

B. Hardware description

1) Sensor board: The sensor board consists in an IMU with MEMS sensors, coupled with a network of magnetic sensors. The magnetic field gradient is estimated using a finite-differences algorithm from the magnetic sensor network measurements and known positions of sensitive elements. In the following, it is assumed that sensors provide sampled measurements.

2) Measurement sampling model: Inertial and magnetic measurements are synchronously sampled by $\Sigma - \Delta$ analog to digital converters at a frequency $1/T$, with $T = 3.072$ms. The effect of analog to digital conversion can be modelled as a weighted integration or a convolution. Let us denote m_{IMU} and m_{MAG} two convolution fonctions. The relationship between sampled measurements provided by the sensor board and continuous-time variables can then be modelled by:

- $\boldsymbol{\omega}_b[k] = (m_{\mathrm{IMU}} \star \boldsymbol{\omega}_b)(kT)$
- $\boldsymbol{\gamma}_b[k] = (m_{\mathrm{IMU}} \star \boldsymbol{\gamma}_b)(kT)$
- $\mathbf{B}_b[k] = (m_{\mathrm{MAG}} \star \mathbf{B}_b)(kT)$

where $\star$ stands for convolution. In previous lines, m_{IMU} and m_{MAG} are functions of the time variable, that depend on ADC settings and on the programmation of an onboard microcontroller.

C. Performance criteria

Contrary to fingerprinting approaches, no assumption is made in our model regarding the relationship between the magnetic field and location. Therefore we can only estimate a translation vector, whose estimation is subject to drifting. Our performance criteria will then represent the drifting error relative to the estimated travelled distance.

If $\hat{\mathbf{x}}[k]$ is the estimate of the translation vector $\mathbf{x}[k]$ at time kT, denoting $d[k]$ the estimated travelled distance at time kT recursively defined as

$$d[k+1] \triangleq d[k] + \|\hat{\mathbf{x}}[k+1] - \hat{\mathbf{x}}[k]\|$$

with $d[0] \triangleq 0$, we define the drifting error at time-step k with respect to time-step k_0 as:

$$\epsilon[k, k_0] = \frac{\|(\hat{\mathbf{x}}[k] - \hat{\mathbf{x}}[k_0]) - (\mathbf{x}[k] - \mathbf{x}[k_0])\|}{d[k] - d[k_0]} \tag{6}$$

This drifting error can be expressed as a percentage of estimated travelled distance. Whenever it is known that $\mathbf{x}[k] - \mathbf{x}[k_0] = 0$, that is to say the trajectory from k_0 to k is a closed path, $\epsilon[k, k_0]$ expresses a relative error which depends only on estimated outputs:

$$\epsilon[k, k_0] = \frac{\|(\hat{\mathbf{x}}[k] - \hat{\mathbf{x}}[k_0])\|}{d[k] - d[k_0]} \tag{7}$$

This closed path criteria will be used whenever no external position reference is available.

III. Proposed EKF observer

In the following, we describe an Extended Kalman Filter (EKF) providing a motion estimate.

A. Partial discrete-time uncertain model

Let us denote $q[k] = q(kT)$, $\mathbf{v}_b[k] = \mathbf{v}_b(kT)$ and $\mathbf{x}_i[k] = \mathbf{x}_i(kT)$. Let us denote the discrete-time partial state vector including the stationary component of the magnetic field:

$$x^{(\mathrm{s})}[k] = (q[k], \mathbf{v}_b[k], \mathbf{x}_i[k], \mathbf{B}_b[k])$$

Let $\hat{u}[k]$ be an m dimensional real vector of known sampled noisy inertial and magnetic measurements, and $u[k]$ their unknown denoised counterpart, with $Q_u = \mathrm{Cov}(u - \hat{u}, u - \hat{u})$. In the following, we assume that at each time step, we know $f^{(\mathrm{s})}$ and $g_k^{(\mathrm{s})}$ such that:

$$\begin{aligned} x^{(\mathrm{s})}[k+1] =& f^{(\mathrm{s})}(x^{(\mathrm{s})}[k], u[k]) + \nu_k^{(\mathrm{s})} \\ =& f^{(\mathrm{s})}(x^{(\mathrm{s})}[k], \hat{u}[k]) \\ &+ g_k^{(\mathrm{s})}(x^{(\mathrm{s})}[k])(u[k] - \hat{u}[k]) + \nu_k^{(\mathrm{s})} \end{aligned} \tag{8}$$

where

$$\begin{aligned} g_k^{(\mathrm{s})}(x^{(\mathrm{s})}[k])(\alpha) &\triangleq \left(\frac{\partial f_k^{(\mathrm{s})}(x^{(\mathrm{s})}[k], \hat{u}[k])}{\partial \alpha} \right) \alpha \\ &\triangleq G_k \alpha \end{aligned}$$

and $\nu_k^{(\mathrm{s})}$ is a zero mean gaussian variable. Equation (8) represents the discrete-time version of equations (1-3,5).

B. Power-line interference model

Power-line interference (denoted $\mathbf{B}^{(\mathrm{pl})}$) violates the assumption that the total magnetic field be time-invariant in the inertial frame. It creates an oscillating velocity estimation error, and hinders filter tuning. Therefore, we include the discrete-time power-line perturbation model described in [21] into our discrete-time model. In $\mathfrak{R}_i$, denoting $\mathbf{B}_i^{(\mathrm{pl})}[k] = (m_{\mathbf{B}} \star \mathbf{B}_i^{(\mathrm{pl})})(kT)$, $\mathbf{B}_i^{(\mathrm{pl})}[k]$ can be modelled with the following recursion:

$$\begin{aligned} &\mathbf{B}_i^{(\mathrm{pl})}[k+1] + \mathbf{B}_i^{(\mathrm{pl})}[k-1] \\ &= 2\cos(\omega_0)\mathbf{B}_i^{(\mathrm{pl})}[k] + \nu_k^{(\mathrm{pl})} \end{aligned} \tag{9}$$

with $\omega_0 = 2\pi f_0 / f_s$, where f_0 and $f_s \triangleq 1/T$ are the power line interference and sampling frequencies respectively.

This leads us to add the following linear dynamic into our model:

$$x^{(\mathrm{pl})}[k+1] = F^{(\mathrm{pl})} x^{(\mathrm{pl})}[k] + \begin{pmatrix} \nu_k^{(\mathrm{pl})} \\ 0 \end{pmatrix} \tag{10}$$

where

$$F^{(\mathrm{pl})} \triangleq \begin{pmatrix} 2\cos(\omega_0) I_3 & -I_3 \\ I_3 & 0 \end{pmatrix}$$

with I_3 denoting the (3x3) identity matrix, so that:

$$x^{(\mathrm{pl})}[k+1] = \begin{pmatrix} \mathbf{B}_i^{(\mathrm{pl})}[k+1] \\ \mathbf{B}_i^{(\mathrm{pl})}[k] \end{pmatrix} \tag{11}$$

Neglecting the effect of movement on the measurement of power-line interference while sampling, the measurement model of the magnetic field at step k becomes a sum of $\mathbf{B}[k]$ (time-invariant in $\mathfrak{R}_i$) and $\mathbf{B}^{(\mathrm{pl})}[k]$ (space-invariant in $\mathfrak{R}_i$).

Our uncertain discrete model reads now:

$$\begin{aligned} x[k+1] &\triangleq \begin{pmatrix} x^{(\mathrm{s})}[k+1] \\ x^{(\mathrm{pl})}[k+1] \end{pmatrix} \\ &\triangleq f_k\left(x[k], u[k]\right) + g_k(x[k])(u[k] - \hat{u}[k]) + \nu_k \end{aligned} \tag{12}$$

with ν_k a zero mean gaussian variable of covariance matrix Q.

C. EKF Implementation

The EKF consists in several classic steps [1, Sec. 8.2]:

State prediction. Evaluates the approximate discrete-time model (12), from Sec. III-B. Denoting $\hat{x}^+$ the state estimate and $\hat{x}^-$ the predicted state before state and covariance update:

$$\hat{x}^-[k+1] = f_k(\hat{x}^+[k], \hat{u}[k])$$

State covariance prediction. Denoting $\tilde{x}^- \triangleq \hat{x}^- - x$ the prediction error where x is the actual state, denoting F the Jacobian matrix of $f_k(\square, \hat{u}[k])$, state covariance is predicted using the linearized error model:

$$\begin{aligned} \tilde{x}^-[k+1] \approx\ & F_k \tilde{x}^+[k] \\ &+ g_k(x[k])(u[k] - \hat{u}[k]) + \nu_k \end{aligned}$$

Denoting P^- and P^+ state-covariance matrices respectively before and after update, with Q_u and R_k chosen so as to represent known or hypothesized uncertainties about sensor measurements[2], while Q is a covariance matrix modeling uncertainties about the uncertain discrete-time model itself[3], we have:

$$P^-[k+1] = F_k P^+[k] F_k^T + G_k Q_u G_k^T + Q \tag{13}$$

Measurement prediction. The following magnetic measurement model is used:

$$\begin{aligned} z_{\mathbf{B}_b}[k] &\triangleq h_k(x[k]) + \nu_{z_{\mathbf{B}_b}} \\ &= \mathbf{B}_b[k] + q[k]^{-1} * \mathbf{B}_i^{(\mathrm{pl})}[k] * q[k] + \nu_{z_{\mathbf{B}_b}} \end{aligned}$$

[2] these are essentially measurement noise covariances.

[3] chosen as zero except for power line interference filtering

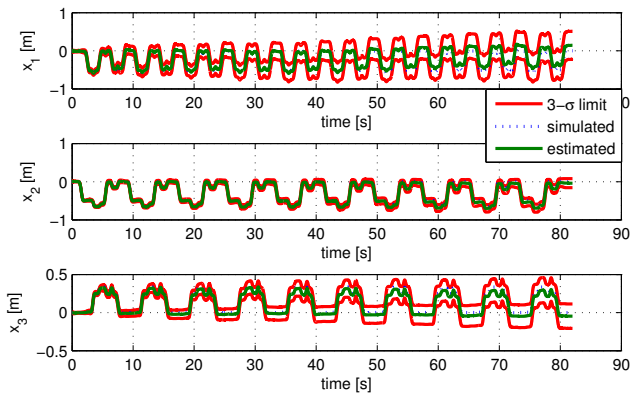


Fig. 1. Simulation: comparison between simulated and estimated positions in cartesian coordinates. 3-σ limits estimated by the filter are drawn in red.

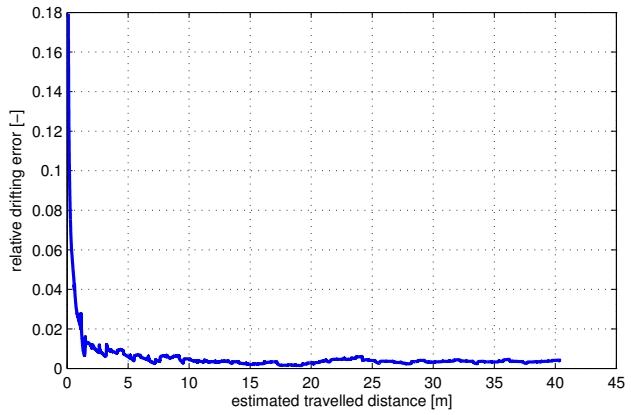


Fig. 2. Simulation: drifting error relative to the travelled distance.

State and covariance update in this case using solely magnetic field measurements, with classic Kalman filter formulas:

$$\begin{aligned}\hat{x}^+[k+1] &= \hat{x}^-[k] + L_k\left[z[k] - h_k(\hat{x}^-[k])\right]\\ L_k &= P^-[k]H_k\Omega_k^{-1}\\ \Omega_k &= H_k^T P^-[k]H_k + R_k\end{aligned}$$

$$\begin{aligned}P^+[k] &= P^-[k]\\ &- P^-[k]H_k\left[H_k^T P^-[k]H_k + R_k\right]^{-1}H_k^T P^-[k]\end{aligned}$$

with H_k being the Jacobian of the measurement function h_k, R_k the measurement covariance matrix at step k, L_k is the Kalman gain and Ω_k the innovation covariance.

IV. Simulation

The Extended Kalman Filter described above is implemented in MATLAB. For testing purposes, we generate a trajectory, and simulate corresponding sensor measurements. The magnetic field is simulated to best fit the earth magnetic field in SYSNAV (Vernon, FRANCE), with typical perturbations found in an office building, and power-line interference typically observed near the Vernon train station.

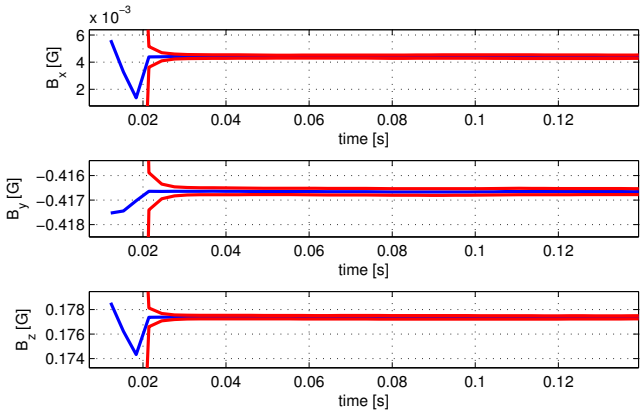


Fig. 3. Simulation: stationnary component of the magnetic field as estimated by the EKF at initialisation (blue). Red lines represent 3-σ limits.

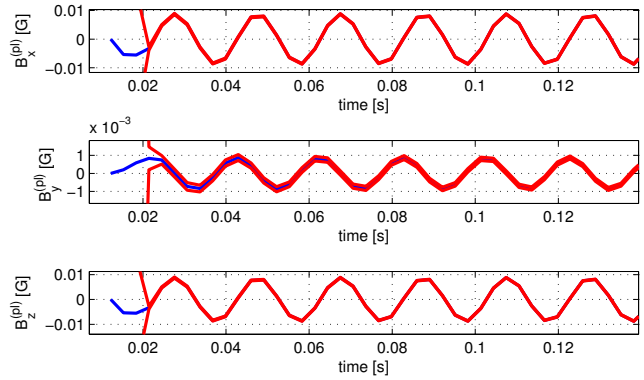


Fig. 4. Simulation: 50Hz component of the magnetic field as estimated by the EKF at initalisation (blue). Red lines represent 3-σ limits.

It is modelled as the sum of a constant field, a set of random magnetic dipoles, and a 50Hz periodic oscillation (amplitude $\sim$14mG).

The simulated trajectory consists in 8 mouvements along the edges of a 50cm cube in various orientations. The whole sequence is repeated 10 times. The estimated trajectory is shown (Fig. 1), and the criteria (Fig. 2) evaluated with respect to the initial position.

In this example, after an initial drift due to the power-line interference being filtered, the drifing error remains under 1% of estimated travelled distance (Fig. 2). The final 3-σ confidence intervals are $x_1 \in [-0.22m, 0.56m]$, $x_2 \in [-0.12m, 0.08m]$, $x_3 \in [-0.16m, 0.10m]$ (Fig. 1), while the final position is zero, within each interval. In practice, the observed drift increases with the magnitude of the state derivatives. Power-line is cancelled in few time-steps after initialisation (Fig. 4), leaving undisturbed the estimate of the stationnary component of the magnetic field (Fig. 3).

The designed EKF works as expected on simulated data, effectively cancelling power-line interference while yielding a small drifting error.



Fig. 5. Experimental setup: the sensor board is carried by hand in SYSNAV's office

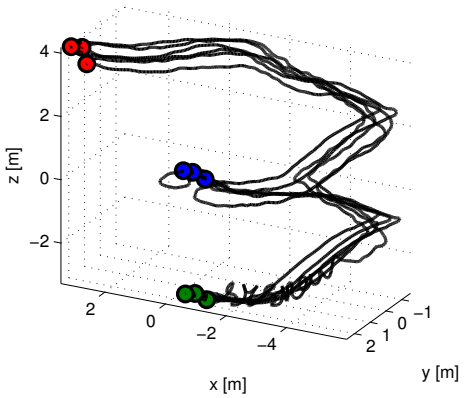


Fig. 6. Experimental: Indoor trajectory between 3 landmarks on different floors, reconstructed from experimental data

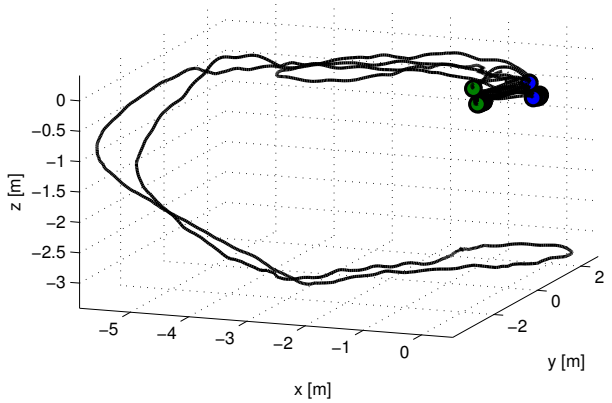


Fig. 7. Experimental: Indoor trajectory between 2 landmarks on a desk, from experimental data

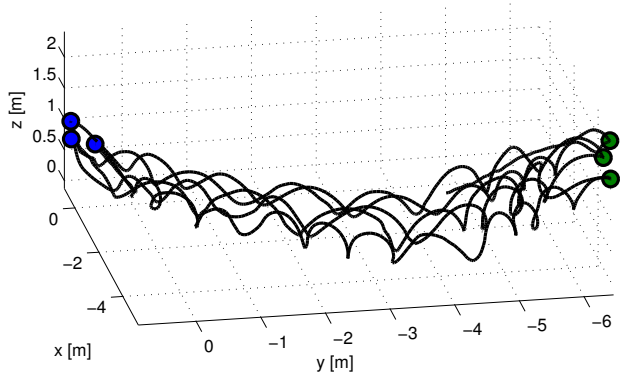


Fig. 8. Experimental: Indoor trajectory between 2 landmarks, from experimental data

V. Experimental results

The proposed navigation solution is tested in SYSNAV's office, with the sensor board carried by hand as shown in Fig. 5. From there, 3 landmarks are chosen in the building on different floors, and the prototype is layed on top of each 3 times. The reconstructed path is shown in Fig. 6. All 9 computable closed path relative drift errors (7) in this test lay between 0.57 and 0.79%. In another test, 2 landmarks are chosen $\sim$1.2m apart on the same desk, and the prototype is layed on top of each 8 times, with one loop on the floor below. The reconstructed path is shown in Fig. 7. All 56 computable closed path drift errors in this test lay between 0.28 and 2.84%. In a third test, the system is moved around and layed on top of 2 landmarks 3 times each. The reconstructed path is shown in Fig. 8. All 6 computable closed path drift errors in this test lay between 0.89% and 1.79%.

The system is given to different users who do not know the system. They are asked to chose at least 2 landmarks, and travel in a closed path repeatedly between them as many times as they want. They are free to chose any path they want in between their chosen landmarks. Closed path relative drift errors are made on the 14 additional different trajectories thereby obtained. The resulting distribution of computed errors over all these tests is reported in an histogram in Fig. 9: computable relative drift errors all lay between 0.13% and 3.3% of travelled distance, the majority laying under 2%, which is a level of performance comparable with pedestrian dead-reckoning systems' [13], [17].

Conclusion

The motion of a rigid body equipped with inertial and magnetic sensors has been modeled. A reduced EKF observer has been designed to estimate the attitude and the position of the rigid body in presence of measurement noise. Some numerical simulations have been carried out to illustrate the obtained convergence. Finally a large series of experiments

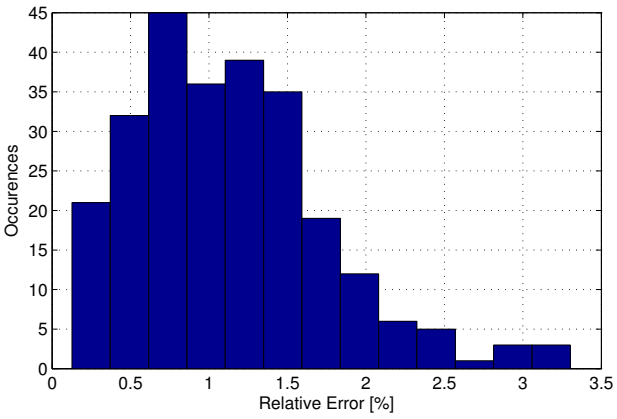


Fig. 9. Experimental closed path relative error occurrences

has been performed to show how effective this approach is on real applications. To be more specific, on the considered indoor navigation experiments, using distributed magnetometry with inertial sensors yields a closed path drift error of the designed observer smaller than a maximum of 3.3% of travelled distance.

This work lets open some questions. Further research is needed in order to extend experimental results in various building environments, and improve high dynamic performance. Other performance criteria may be considered to focus on the observer transient response, and on the accuracy of attitude estimates.

REFERENCES

[1] B. D.O. Anderson and J.B. Moore. *Optimal filtering*. Dover Books on Electrical Engineering. Mineola, N.Y., Dover Publications, 2005.

[2] P. Batista, N. Petit, C. Silvestre, and P. Oliveira. Further results on the observability in magneto-inertial navigation. In *American Control Conference (ACC)*, pages 2503–2508, Washington DC, 2013.

[3] A.H. Brodtkorb, A.R. Teel, and A.J. Sorensen. Sensor-based hybrid observer for dynamic positioning. In *IEEE 54th Annual Conference on Decision and Control*, pages 948–953, Osaka, Japan, 2015.

[4] J. Chung, M. Donahoe, C. Schmandt, I.-J. Kim, P. Razavai, and M. Wiseman. Indoor location sensing using geo-magnetism. In *9th international conference on Mobile systems, applications, and services (MobiSys)*, pages 141–154, Washington DC, 2011.

[5] G. Deak, K. Curran, and J. Condell. A survey of active and passive indoor localisation systems. *Computer Communications*, 35(16):1939–1954, 2012.

[6] E. Dorveaux. *Magneto-inertial navigation: principles and application to an indoor pedometer*. PhD thesis, Ecole Nationale Supérieure des Mines de Paris, 2011.

[7] E. Dorveaux, T. Boudot, M. Hillion, and N. Petit. Combining inertial measurements and distributed magnetometry for motion estimation. In *American Control Conference (ACC)*, pages 4249–4256, San Francisco, CA, 2011.

[8] E. Dorveaux and N. Petit. Presentation of a magneto-inertial positioning system: navigating through magnetic disturbances. In *International Conference on Indoor Positioning and Indoor Navigation (IPIN)*, Guimaraes, 2011.

[9] N. Fallah, I. Apostolopoulos, K. Bekris, and E. Folmer. Indoor human navigation systems: A survey. *Interacting with Computers*, 25:21–33, 2013.

[10] E. Foxlin. Pedestrian tracking with shoe-mounted inertial sensors. *Computer Graphics and Applications*, 25(6):38–46, 2005.

[11] S. Gros and M. Diehl. Attitude estimation based on inertial and position measurements. In *IEEE 51st Annual Conference on Decision and Control*, pages 1758–1763, Maui, HI, 2012.

[12] R. Harle. A survey of indoor inertial positioning systems for pedestrians. *Commun. Surv. Tutorials*, 15(3):1281–1293, 2013.

[13] A.R. Jimenez, F. Seco, C. Prieto, and J. Guevara. A comparison of pedestrian dead-reckoning algorithms using a low-cost MEMS IMU. In *IEEE International Symposium on Intelligent Signal Processing (WISP)*, pages 37–42, Budapest, 2009.

[14] H. Koyuncu and S. H. Yang. A survey of indoor positioning and object locating systems. *International Journal of Computer Science and Network Security*, 10(5):121–128, 2010.

[15] R. Mautz. Overview of current indoor positioning systems. *Geodesy and Cartography*, 35(1):18–22, 2009.

[16] R. Mautz and S. Tilch. Survey of optical indoor positioning systems. In *International Conference on Indoor Positioning and Indoor Navigation (IPIN)*, pages 1–7, Guimaraes, 2011.

[17] J.-O. Nilsson, I. Skog, and P. Handel. Performance characterisation of foot-mounted ZUPT-aided INSs and other related systems. In *International Conference on Indoor Positioning and Indoor Navigation (IPIN)*, pages 1 – 7, Zurich, 2010.

[18] L. Ojeda and J. Borenstein. Non-GPS navigation for security personnel and first responders. *J. Navigation*, 60(03):391–407, 2007.

[19] N. Praly, P-J Bristeau, J. Laurent-Varin, and N. Petit. Using distributed magnetometry in navigation of heavy launchers and space vehicles. In *Progress in Flight Dynamics, Guidance, Navigation, Control, Fault Detection, and Avionics*, volume 6, pages 45–54. EDP Sciences, 2013.

[20] A. Roberts and A. Tayebi. On the attitude estimation of accelerating rigid-bodies using GPS and IMU measurements. In *50th IEEE Conference on Decision and Control and European Control Conference*, pages 8088–8093, Orlando, FL, 2011.

[21] R. Sameni. A linear Kalman notch filter for power-line interference cancellation. In *16th CSI International Symposium on Artificial Intelligence and Signal Processing*, pages 604–610, Shirez, Iran, 2012.

[22] S. Shahidi and S. Valaee. Gipsy: Geomagnetic indoor positioning system for smartphones. In *International Conference on Indoor Positioning and Indoor Navigation (IPIN)*, pages 1–7, Banff, AB, 2015.

[23] I. Skog, J.-O. Nilsson, and P. Handel. Evaluation of zero-velocity detectors for foot-mounted inertial navigation systems. In *International Conference on Indoor Positioning and Indoor Navigation (IPIN)*, 2010.

[24] W. Storms, J. Shockley, and J. Raquet. Magnetic field navigation in an indoor environment. *Ubiquitous Positioning Indoor Navigation and Location Based Service*, pages 1–10, 2010.

[25] J.F. Vasconcelos, C. Silvestre, and P. Oliveira. A nonlinear GPS/IMU based observer for rigid body attitude and position estimation. In *IEEE Conference on Decision and Control*, pages 1255–1260, Cancun, Mexico, 2008.

[26] B. Vik and T.I. Fossen. A nonlinear observer for GPS and INS integration. In *40th IEEE Conference on Decision and Control*, volume 3, pages 2956–2961, Orlando, FL, 2001.

[27] D. Vissière, A. Martin, and N. Petit. Using distributed magnetometers to increase imu-based velocity estimation into perturbed area. In *Conference on Decision and Control (CDC)*, pages 4924–4931, New Orleans, LA, 2007.

[28] D. Vissiere, A. Martin, and N. Petit. Using magnetic disturbances to improve imu-based position estimation. In *European Control Conference (ECC)*, pages 2853–2858, Kos, 2007.

[29] D. Vissière, A. Martin, and N. Petit. Système fournissant la vitesse et la position d'un corps en utilisant les variations du champ magnétique évaluées grâce aux mesures de un ou des magnétomètres et de une ou des centrales inertielles. *Patent FR2914739 (A1)*, 2008.